

# Reconfigurable Surfaces Using Fringing Electric Fields from Nanostructured Electrodes in Nematic Liquid Crystals

Rami Ghannam,\* Yuanjie Xia, Dezhi Shen, F. Anibal Fernandez, Hadi Heidari, and Vellasaimy A. L. Roy

Liquid crystals with a varying phase profile enable reconfigurable and intelligent devices to be designed, which are capable of manipulating incident electromagnetic fields in display, telecommunications as well as wearable applications. The active control of defects in these devices is becoming more important, especially since the electrodes used to manipulate them are shrinking to nanometer length scales. In this paper, a simple subwavelength, 1D, interdigitated metal electrode structure that can be reconfigured using nematic liquid crystals aligned in the homeotropic, planar, and hybrid methods are demonstrated. Accurate electro-optic modeling of the directors and the defects are shown, which are induced by the fringing electric fields. Applied voltages result in liquid crystal reorientation near the bottom surface, such that defects are induced between the electrodes. The height of the electrodes does not affect the lateral position of these defects. Rather, this can be achieved by increasing the biasing voltage on the top electrode, which also leads to greater splay-bend in the bulk of the material. These results therefore aim to generalize the control of defects in complex anisotropic nematic liquid crystals using simple interdigitated structures for a range of reconfigurable intelligent surface applications.

## 1. Introduction

Liquid crystals (LCs) are a soft state of matter that exhibit flow properties similar to liquids yet the molecules maintain weak positional and orientational ordering, which allows them to have physical properties that are similar to solids.

The most common application of nematic liquid crystals (NLCs) is in liquid crystal displays (LCDs). Such light modulation devices have evolved from regular displays found on

wrist-watches and pocket-calculators to more sophisticated non-display photonic devices<sup>[1]</sup> such as real-time holograms,<sup>[2,3]</sup> all-optical interconnects,<sup>[4]</sup> optical tweezers,<sup>[5]</sup> and many others.<sup>[6]</sup> Most recently, they have been used to control magnetic microbots,<sup>[7]</sup> for terahertz beam-steering applications<sup>[8]</sup> and for an artificial iris application.<sup>[9,10]</sup> In all such light-modulation applications, liquid crystals (LCs) were switched from an initial state, which is determined by an alignment process, to a final equilibrium-state. This final state was based on an external electric field, which causes the LCs to re-align themselves.<sup>[11]</sup> Such electric fields are generated from an array of conducting electrodes, which translate electrical information into optical data through the LC medium.<sup>[12]</sup>

The aim of this paper is therefore to demonstrate and generalize findings regarding the use of fringing electric fields from nanostructured electrodes for switching liquid crystals. In particular, we focus on their application to reconfigure or redirect electromagnetic waves in the visible spectrum. For example, similar to the wearable contact lens application mentioned by De Smet et al.<sup>[13]</sup> and Quiñero et al.,<sup>[9]</sup> they can be intelligently switched to block wavelengths of light that cause epilepsy, a condition known as photosensitive epilepsy (PSE).<sup>[14]</sup> In fact, instead of using conventional colored eye glasses,<sup>[15]</sup> we believe that future contact lenses can be designed to prevent this condition, especially since flexible electronics have been successfully integrated on soft contact lenses.<sup>[16]</sup>

In typical display applications where liquid crystal materials have traditionally been used, electrodes were designed to avoid the formation of defects or disclinations,<sup>[17]</sup> since they cause a degradation in image quality. However, thanks to advancements in nanotechnology and micro-fabrication, the shrinking size of these electrodes and the overall devices is bound to induce defects that are caused by strong fringing electric fields. These defects are therefore becoming more important in such sub-wavelength devices. Consequently, we aim to show how these defects are formed for different electrode designs and what voltages are necessary to cause them. This is particularly important if we need to understand how these surfaces can be used for intelligent applications.

The use of metallic interdigitated (IDT) electrodes in homeotropically aligned LCs were first reported in ref. [18]. These were

R. Ghannam, Y. Xia, H. Heidari, V. A. L. Roy  
James Watt School of Engineering  
University of Glasgow  
Glasgow G12 8QQ, UK  
E-mail: rami.ghannam@glasgow.ac.uk

D. Shen, F. A. Fernandez  
Department of Electronic and Electrical Engineering  
University College London  
London WC1E 7JE, UK

© 2021 The Authors. Advanced Theory and Simulations published by Wiley-VCH GmbH. This is an open access article under the terms of the Creative Commons Attribution License, which permits use, distribution and reproduction in any medium, provided the original work is properly cited.

DOI: 10.1002/adts.202100058

used for measuring flexoelectricity in NLCs. However, initial observations of disclinations due to IDT electrodes in homeotropically aligned NLCs were first reported by ref. [19]. Lindquist et al. described the presence of “defect walls” between the electrodes when the cell was placed between crossed polarisers. Certainly, light can be extinguished in this region, but that is not solely due to the presence of a defect. We therefore aim to show how the electrode topological pattern, the alignment method and the applied voltage influence defect nucleation and optical behaviour in these devices using experimentally verified simulations. In some telecommunications and display applications, inducing defects in liquid crystal materials is desirable to ensure that a sharp phase profile is obtained. For example, this might be particularly important to obtain a high diffraction efficiency.<sup>[20]</sup>

The remainder of the paper is organised as follows: first, we will provide a review of recent developments in using IDT electrodes for the manipulation of NLCs. Next, we will describe our methodology in simulating our LC devices. Subsequently, we will present our findings in reconfiguring NLCs from three different initial states using both optical and LC director profile data.

### 1.1. State of the Art

In this section, we describe recent advances in controlling LCs using IDT electrodes. In fact, simple and periodic IDT electrodes have often been used for beam steering applications. These periodic diffraction grating structures have gained interest due to their flexibility in controlling light propagation in comparison to prisms.<sup>[21]</sup> They are generally regarded as one of the most important devices in the development of several fields of science.<sup>[20]</sup> Therefore, LCs have been used for this purpose, since they can be tuned and reconfigured using external stimuli such as an electric field. For example, a tunable diffraction grating was demonstrated by Habibpourmoghadam et al.<sup>[22]</sup> Moreover, a homeotropically aligned NLC cell with IDT electrodes was demonstrated by Choi et al. to switch between opaque and transparent states for window and display applications.<sup>[23–25]</sup> Furthermore, to improve the switching speed of homeotropic LC devices while maintaining a high phase retardation ( $\Delta\phi$ ), Simdyankin et al. argued that decreasing electrode spacings in IDTs was a better solution instead of reducing cell thickness, since it maintains a high phase retardation.<sup>[26]</sup> Moreover, the diffraction efficiency of fringing electric fields from IDTs has recently been reported by Chen et al. for a planar aligned LC cell.<sup>[27]</sup> Their findings in ref. [27] show how the rubbing direction influences the switching speed of a planar aligned transparent cell with IDT electrode width  $w = 2.8 \mu\text{m}$ , electrode gap  $l = 6 \mu\text{m}$ , and cell gap  $d = 3.4 \mu\text{m}$ . Their findings also show a variation in diffraction angle due to a change in the applied voltage. Further, planar aligned LC cell with IDT electrodes was demonstrated in ref. [28]. The reader is also referred to ref. [21] for a thorough review of LCs used in diffraction gratings.

In all these previous investigations, the occurrence of defects due to both the electrode profile and the electric field were not fully reported. However, these defects will influence the switching properties of the cell. Understanding and being able to predict the occurrence of these defects could help in designing better diffraction gratings, such as sharp phase profiles for

blazed grating applications. In fact, the surface profile of micro-patterned electrodes have shown to align NLCs in the literature using simulation and experimental data.<sup>[29,30]</sup> Therefore, we aim to show the effect of topographic gratings and LC switching. Moreover, we aim to show the resulting optical patterns that arise from these NLC orientations.

### 1.2. Background and Theory

The orientation of NLCs can be altered by an external electric field. In fact, liquid crystal displays (LCDs) rely on this routine interaction between LCs and the external electric field. Furthermore, due to the anisotropic shape of their molecules, LCs have different dielectric properties that can be expressed in terms of a rank-2 dielectric permittivity tensor,  $\epsilon$ . Moreover, LC alignment can be described in terms of an ensemble average direction of orientation, known as the ‘director’,  $n(x)$ . Here, the Landau de Gennes (LdG) Q-tensor theory was used to determine this alignment, which depends on both orientational order,  $S(x)$ , and a preferred direction of orientation,  $n(x)$ .<sup>[31]</sup> To obtain  $n(x)$ , the total free energy density of the LC material must be minimized. This energy is expressed in terms of the Q-tensor shown in Equation (1), where  $I$  is an identity matrix:

$$Q = S(n \otimes n) - \frac{1}{3}S.I \quad (1)$$

Assuming an elastically isotropic NLC medium, the total free energy density can be described as the sum of the elastic ( $F_{el}$ ), thermotropic ( $F_{th}$ ) and electrostatic energy ( $F_{es}$ ) density functions. The sum of these energy density terms constitutes the bulk free energy density of the liquid crystal,  $F_b = F_{el} + F_{th} + F_{es}$ . Now, applying an electric field to a NLC causes a small amount of charge separation within the molecules, which creates a weak dipole moment. Such dipoles try to arrange themselves in the direction of the field, which causes the directors to align either parallel or perpendicular to the electric field, depending on the dielectric anisotropy of the material,  $\Delta\epsilon = \epsilon_{\parallel} - \epsilon_{\perp}$ , where  $\epsilon_{\parallel}$  and  $\epsilon_{\perp}$  are the dielectric permittivity values in the parallel and perpendicular directions to the director’s optical axis.<sup>[32,33]</sup>

Hence for a displacement field,  $D$ , that is induced by an electric field,  $E$ , the resulting electrostatic energy free density of the NLC is:

$$F_{es} = -\frac{1}{2}\epsilon_0(\epsilon E) \cdot E = -\frac{1}{2}\epsilon_0\epsilon\nabla U \cdot \nabla U \quad (2)$$

where  $U$  is the electric potential and  $E = -\nabla U$ .

Assuming an elastically isotropic NLC medium, the total free energy of the nematic liquid crystal can be stated as follows:

$$F = \int_V \left( \frac{K}{2}\nabla Q^2 + \sigma(Q) - \frac{1}{2}\epsilon_0\epsilon\nabla U \cdot \nabla U \right) dv \quad (3)$$

where  $K$  is the elastic constant and  $\sigma(Q)$  is the thermotropic energy of the liquid crystal, which can be expanded into the following form:

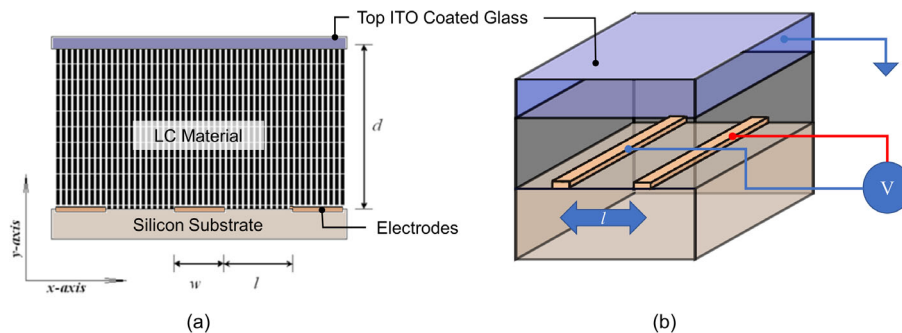


**Figure 1.** Schematic diagram of the LC device. Both the electrode width ( $w$ ) and inter-electrode spacing ( $l$ ) were varied while the thickness of cell gap was kept constant ( $3.5 \mu\text{m}$ ). a) Cross-sectional view of the device. Three different alignment techniques have been investigated, which were homeotropic, planar, and hybrid. b) 3D schematic view of the device.

**Table 1.** Material parameters of the NLCs.<sup>[36–40]</sup>

Parameter	BLO48	5CB
Clearing temperature, $T^*$ [°C]	100	35
Order parameter ( $25^\circ$ )	–	0.65
Order parameter at $\Delta T_{NI}$	–	0.27
$\epsilon_\perp$	5.2	6.7
$\Delta\epsilon$	16.9	13
$n_o(\lambda = 532\text{nm})$	1.573	1.5442
$\Delta n(\lambda = 532\text{nm})$	0.226	0.1918
Splay elastic constant, $K_{11}$ [pN]	15.5	6.4
Twist elastic constant, $K_{22}$ [pN]	12	3
Bend elastic constant, $K_{33}$ [pN]	28	10
Viscosity, $\gamma_1$ [PaS]	0.047	0.0777

$$\sigma(Q) = A \text{tr}(Q^2) + \frac{2B}{3} \text{tr}(Q^3) + \frac{C}{2} \text{tr}Q^4 \quad (4)$$

where  $\text{tr}(\cdot)$  represents the trace of the tensor. Moreover, it was assumed that  $A$  is a temperature dependent coefficient,  $A = a(T - T^*) = a\Delta T$  with  $a > 0$ , whereas  $B$  and  $C$  are temperature independent Landau coefficients. For our simulations, these coefficients were set to  $A = -6.5 \times 10^5 \text{Nm}^{-2}$ ,  $B = -16 \times 10^5 \text{Nm}^{-2}$  and  $C = 39 \times 10^5 \text{Nm}^{-2}$ .

The static director configuration can thus be obtained by minimizing the total NLC free energy using the calculus of variations. The Euler–Lagrange minimization procedure helps obtain the equilibrium state of the director profile at a constant electric field. The expressions below are the Euler-Lagrange equations for the liquid crystal bulk free energy, with  $i, j \in x, y$ .

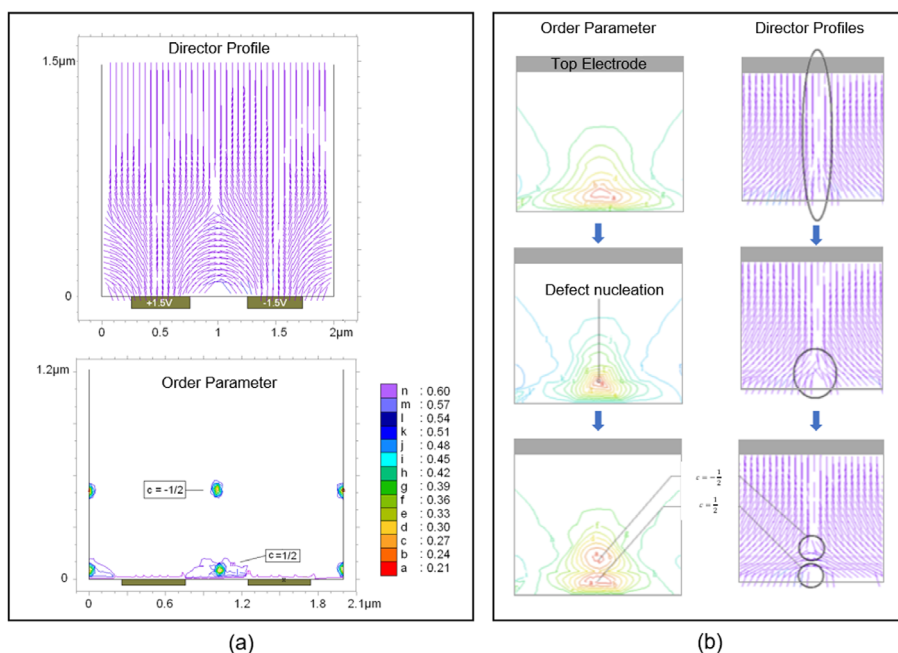


**Figure 2.** Profiles obtained when  $\pm 1.5\text{V}$  were applied to a  $10 \mu\text{m}$  thick device with  $w = l = 0.5 \mu\text{m}$ . a) Top image illustrates a section of the director profile, while the bottom image shows the  $\pm \frac{1}{2}$  defects emerging between the electrodes. The order parameter reduces to almost  $\frac{1}{3}$  its bulk value in the core of the  $\pm \frac{1}{2}$  defects. b) Both the order parameter (on the left) and the director profiles (right) are shown at different time steps in the region between the electrodes. First, a wall defect appears between the electrodes, which separates two regions of different director profiles. This disclination then transforms into two defects of strength  $c = \pm 1$ .

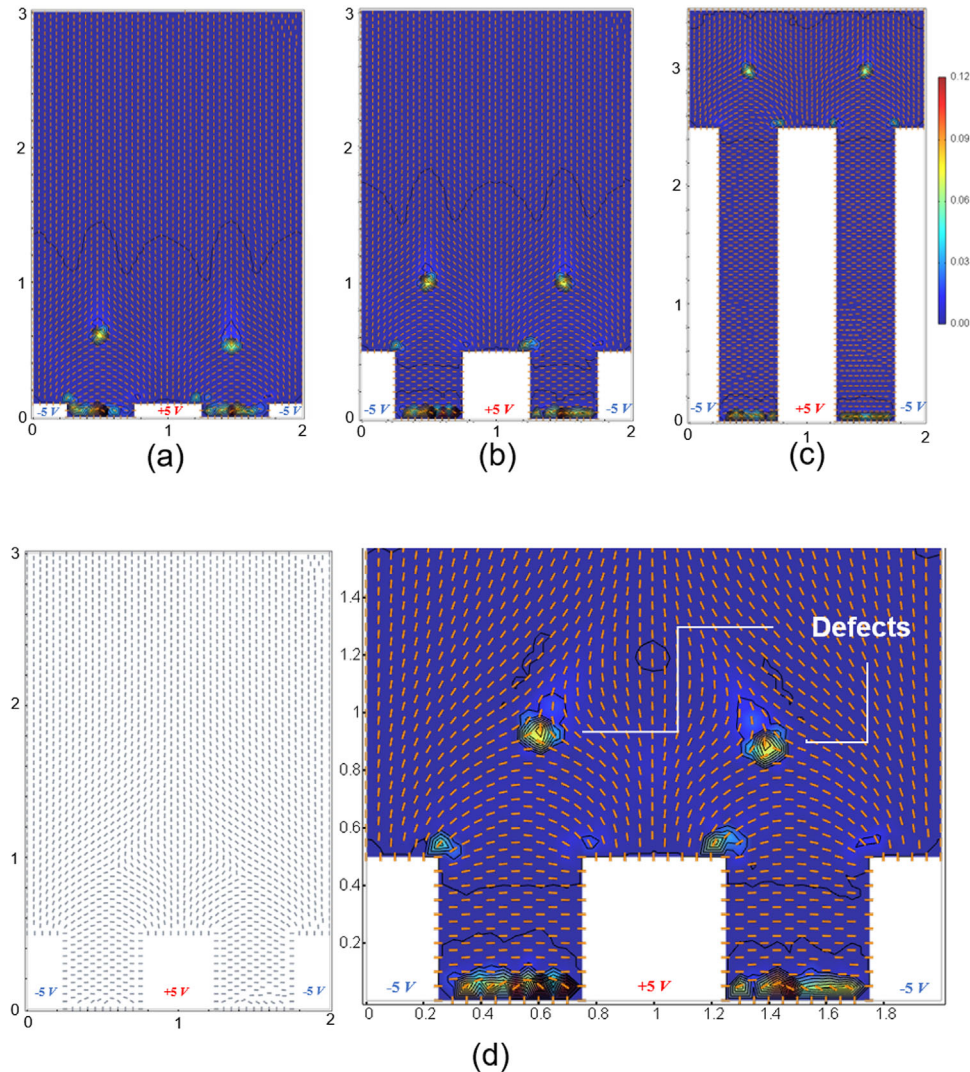


**Figure 3.** Director profile for homeotropic alignment with  $V = \pm 5V$ . All dimensions are in micrometers. a) No bias applied to top electrode. Defects occur between the electrodes near  $x = 0.5 \mu\text{m}$  and  $x = 1.5 \mu\text{m}$ . They are almost  $0.5 \mu\text{m}$  above the electrode surface. This is always the case, regardless of electrode height. In (b) the heights of the electrodes were reduced to  $0.1 \mu\text{m}$ , which did not change the lateral position of the defects, nor did an increase in the electrode height. c) Electrodes are  $h = 2.5 \mu\text{m}$ . Here, more lateral switching occurs between switching, but the position of the defects with respect to the electrode surface is unchanged. d) Bias ( $5V$ ) applied to the top electrode, which results in the defects to move laterally.

$$\frac{\partial}{\partial x_j} \left( \frac{\partial F_b}{\partial Q_{ij}} \right) = \frac{\partial F_b}{\partial Q_i} \quad (5)$$

$$\frac{\partial}{\partial x_j} \left( \frac{\partial F_b}{\partial U_j} \right) = \frac{\partial F_b}{\partial U} \quad (6)$$

## 2. Methodology

A finite element program was used to obtain the director profiles and the order parameter of the NLC material.<sup>[34,35]</sup> A schematic diagram showing a cross sectional area of the liquid crystal device is shown in **Figure 1**. As previously mentioned, 2D simulations

based on the Landau-de Gennes (LdG) Q-tensor theory were used during our investigations. The LC material parameters for 5CB and BL048 liquid crystal mixtures are shown in **Table 1**. Although the elastic constants and viscosity coefficients depend on the temperature, here they are held constant for ease of comparison.

## 3. Results and Discussions

The 2D-director profiles are shown to illustrate the way in which the directors are distorted due to the fringing electric fields. In addition, the S-parameter profiles using the LdG simulations are depicted to accurately identify the position of the defects and to highlight the regions of high direct or distortion, both of which ought to cause a decrease in the order parameter.

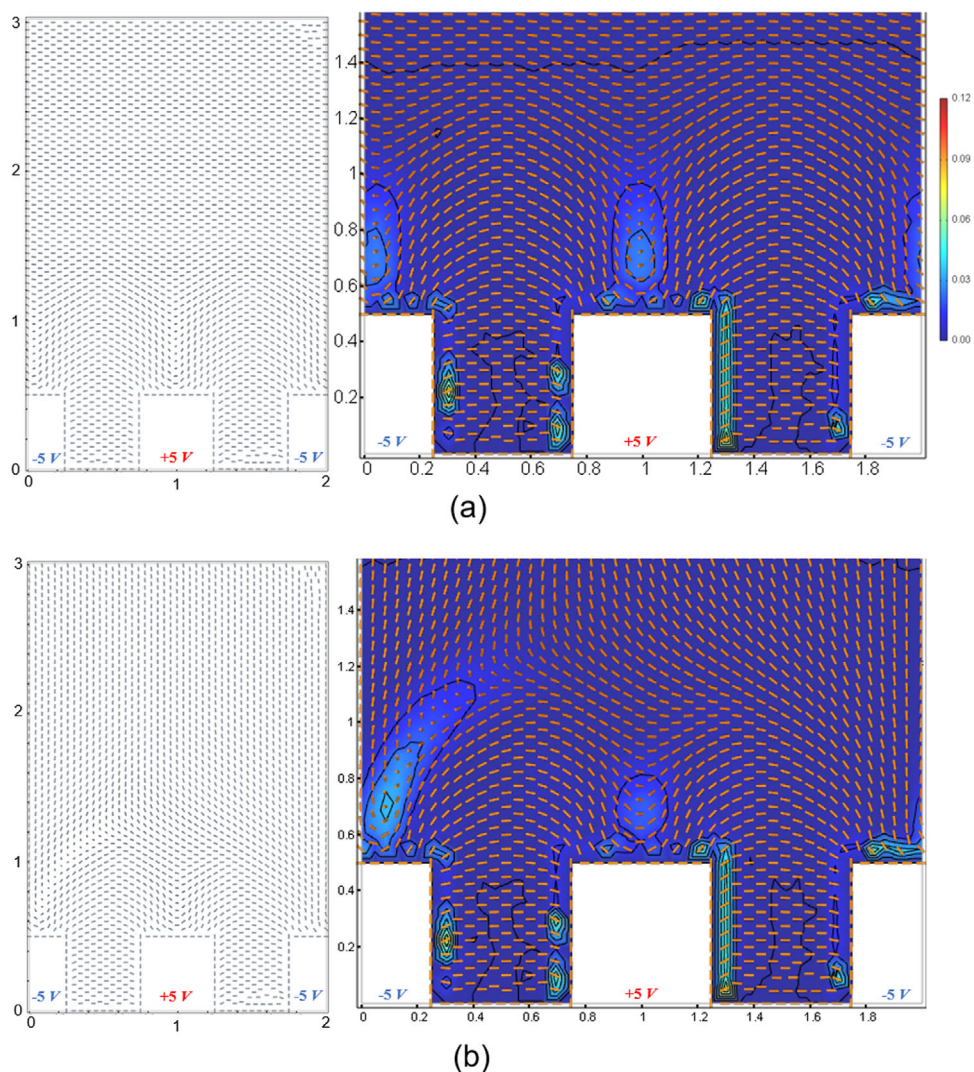


**Figure 4.** Director profile for planar alignment when  $V = \pm 5V$  is applied to the IDT electrodes. All dimensions are in micrometers. a) No bias applied to top electrode. A twist in the directors at the top of the electrodes near  $x = 1 \mu\text{m}$ . b) This twist remains when the bias voltage is increased to  $5V$ . However, there is additional splay-twist in the bulk of the cell.

### 3.1. Homeotropic Alignment

From the simulations, we notice that applying a  $\pm 5V$  results in a defect pair of strength  $\pm \frac{1}{2}$  to emerge between the electrodes. The simulations in **Figure 2** show the formation of these defects. These defects were first observed by Lindquist et al., where  $4 \mu\text{m}$  finger width electrodes were separated via an  $8 \mu\text{m}$  pitch. They reported thick black lines or “defect walls” in the region between the electrodes. As the electrode voltage was increased, the width of the defect wall narrowed and remained stationary. However, this is not the sole reason for the thick black lines to appear between the electrodes, since this is highly dependent on the phase retardation in the cell.

According to our detailed simulations, first, a wall disclination emerges, as shown in **Figure 2a**, which then transform into two point disclinations of strength  $+\frac{1}{2}$  and  $-\frac{1}{2}$ . This process is called “pincement”, which was first noticed by Y. Bouligand.<sup>[31]</sup> These two singularities or “defects” emerge between the electrodes (a

hyperbolic disclination in the bulk of the LC and a parabolic disclination near the surface) as a result of the symmetric voltage pattern. Moreover, increasing the magnitude of the voltage causes the position to these defects to penetrate either upward ( $-\frac{1}{2}$  defect) or downward ( $+\frac{1}{2}$  defect). On the left side of **Figure 2a** is the order parameter, which melts to a value approaching zero. The simulations therefore show the nucleation of a  $\pm \frac{1}{2}$  defect-pair between the electrodes when a symmetric voltage pattern is applied. The final director profile and order parameter are shown in **Figure 2b**.

Varying the electrode height from  $0.1$  to  $2.5 \mu\text{m}$  does not change the lateral position of the defects, as can be seen from **Figure 3a**. The defect is still located  $\approx 0.5 \mu\text{m}$  above the top surface of the electrode. Moreover, increasing the biasing voltage to  $5V$  at the top electrode leads to a lateral movement of the top  $-1/2$  disclination, as shown in **Figure 3b**. In this case, the disclinations move toward the electrodes at  $x = 1 \mu\text{m}$ . It is noteworthy to mention that these steady state director profiles are

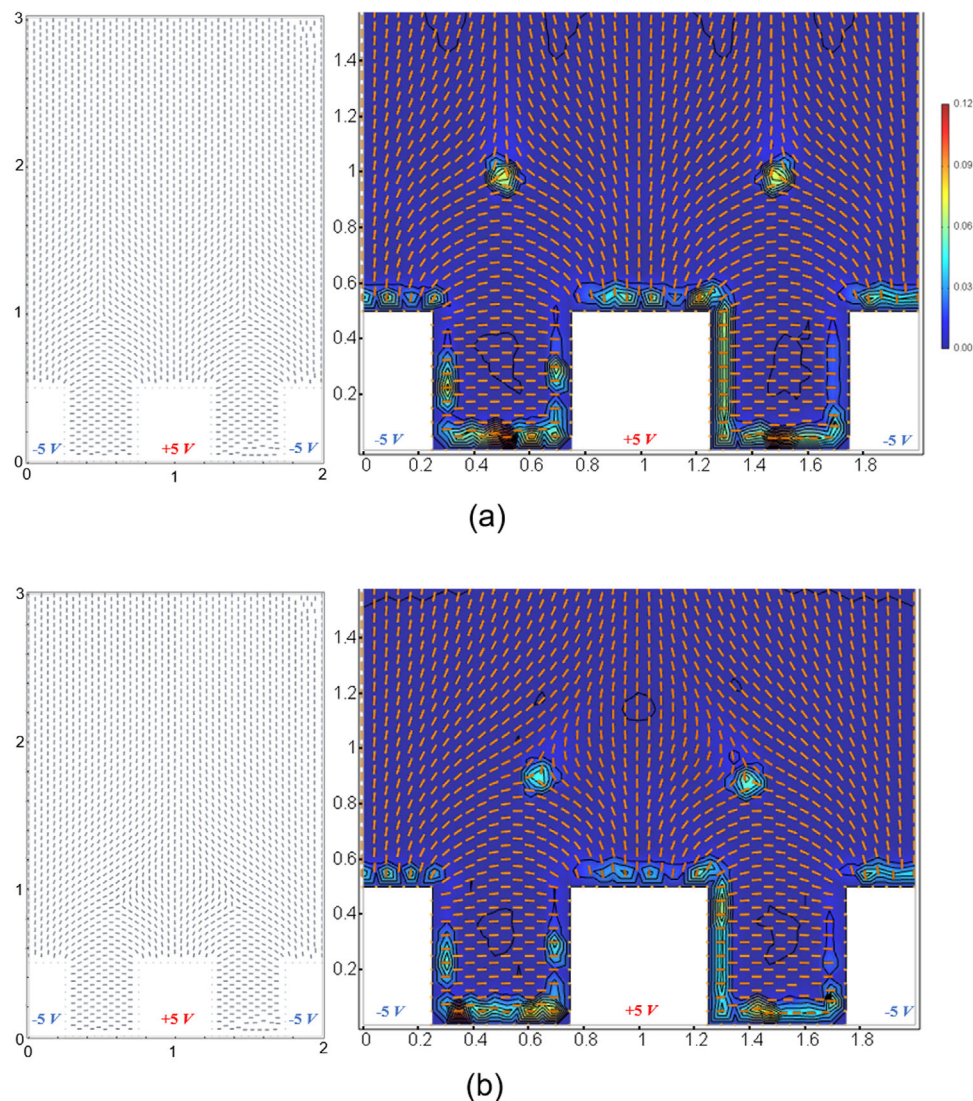


**Figure 5.** Director profile for hybrid alignment when  $V = \pm 5V$ . All dimensions are in micrometers. Similar profiles are obtained to the homeotropic case. a) No bias applied to top electrode, b) bias of 5V applied.

obtained regardless of whether the biasing voltage is applied at the start of the simulations, or after the voltages have been applied.

### 3.2. Planar Alignment

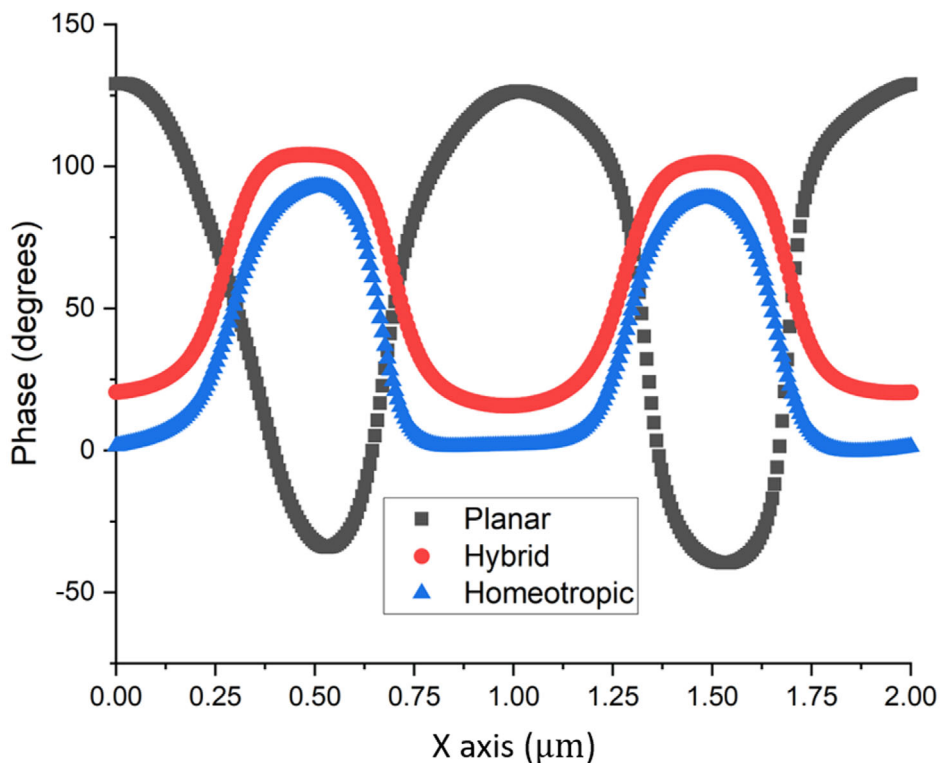
In this case, the LC is aligned parallel to the horizontal  $x$ -direction. When a  $\pm 5V$  is applied to the bottom IDT electrodes, the orientation of the LCs are most prominent above the electrodes resulting in a bend-twist deformation immediately above them. Moreover, no defects appear in this case, as shown from the director profiles in **Figure 4a**. Clearly, the LCs are still predominantly aligned horizontally with no biasing voltage. The magnitude of this perturbation depends on the spacing between the electrodes and the magnitude of the electric field. Larger electrode spacings give rise to electric fields extending further in the

bulk of the cell. However, the magnitude of this field needs to be increased to ensure that the molecules are switched (i.e. greater than the threshold voltage).

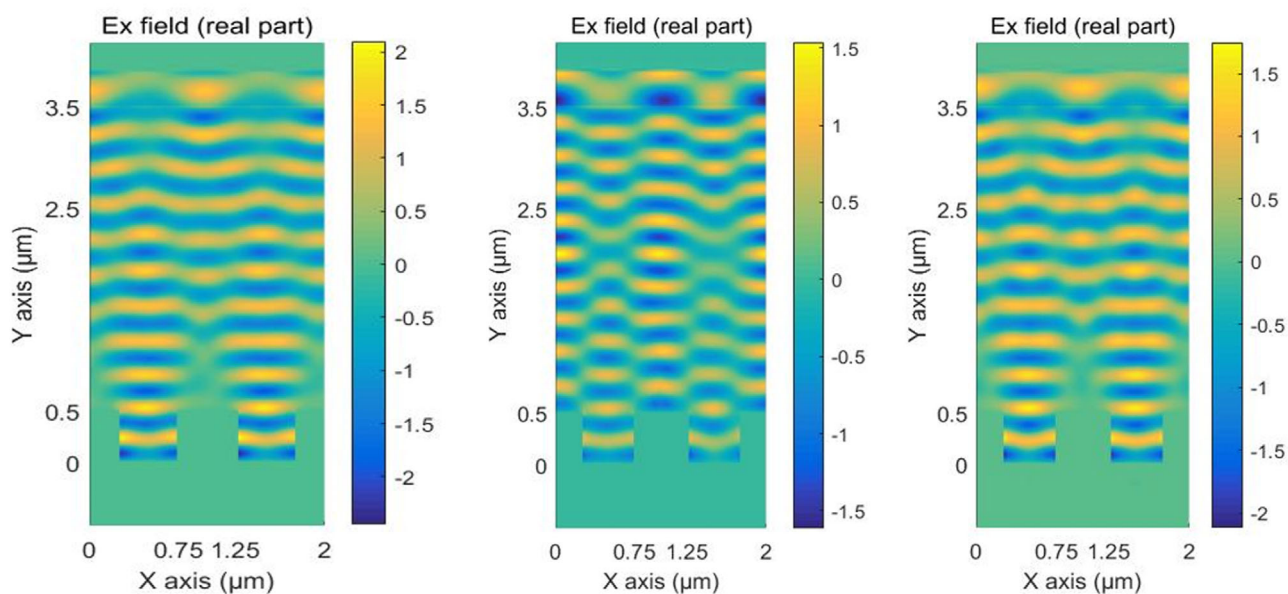
Applying a biasing voltage to the top electrode results in a slight loss of the twisted layer above the electrodes, as shown in **Figure 4b**. Similar to the homeotropic alignment case, the LC in the bulk are now aligned vertically.

### 3.3. Hybrid Alignment

With the hybrid alignment, the LC is aligned differently on the top and bottom layers of the cell. There are two possible options available as shown in **Figure 5**. Choosing homeotropic alignment on the top electrode and in-plane alignment on the bottom electrode results in switching in the region between the electrodes. We also obtain similar director profiles to the homeotropically



(a)



(b)

**Figure 6.** a) Average phase retardation,  $\Delta\phi$  for  $\lambda = 532\text{nm}$ . Both the homeotropic and hybrid alignment cases show similar results, although greater phase retardation can be achieved with homeotropic alignment. Maximum retardation is achieved with planar alignment due to the difference between the initial and final switching states. b) Optical interference through cell in the homeotropic (left), planar (center) and hybrid (right) alignment cases. Maximum transmission can be observed in the region above the central electrode at  $x = 1 \mu\text{m}$  for all three cases.

aligned cells. In both cases, there is a 90° twist instead of a 90° splay-bend. In contrast, homeotropic alignment on the bottom surface and planar alignment on the top leads to similar switching to the planar alignment case. Therefore, LCs are aligned in the direction in plane to the  $\gamma$ -direction of the electrodes. Similar to the homeotropic case, two disclination pairs appear between the electrodes. Applying a biasing voltage to the top electrode again leads to the top disclination pairs to move laterally closer towards the electrodes.

### 3.4. Optics

Figure 6 shows the phase and optical profiles through the cells with different alignments when the biasing voltage on the top electrode is set to zero. Examining the optical phase for normally incident light of wavelength  $\lambda = 532\text{nm}$  shows a hybrid square and sinusoidal profile, with maximum phase retardation reaching  $\pi/2$  in the regions between the electrodes for the homeotropic and hybrid alignment cases. However, maximum phase retardation is achieved with the planar alignment case and this occurs in the region directly above the electrodes. Since these are LCOS devices, which are reflective, light makes a double pass through the cell. In fact, we notice a great deal of destructive interference in the region directly above the electrodes in the homeotropic and hybrid alignment cases. However, in all three cases we notice maximum transmission is obtained in the region above the electrodes.

### 4. Conclusions

We have shown that fringing electric fields generated from electrodes on the bottom substrate of an NLC device change the orientation of the liquid crystal directors. This change in the director orientation results in a distortion of the elastic energy of the NLC material. In addition, the distortion of the elastic energy has been shown to be dependent on the electrodes dimensions. We have shown that director distortion is mainly concentrated in the region between the electrodes. In fact, the induced electric fields have negligible influence on the directors directly above the electrodes. For the homeotropic and hybrid alignment cases, the symmetric voltage pattern only causes director distortion in the region between the electrodes, with little influence in the region directly above the electrodes.

We have shown the nucleation of defects in complex anisotropic nematic liquid crystals using nanoscale electrodes. Controlling these defects is increasingly important for the development of intelligent and reconfigurable devices, which are touted to be a key component in the sixth generation (6G) telecommunications network. Hence, applications of such devices must use the large optical discontinuities that are generated above the electrodes. It was already mentioned in that a large phase retardation can be obtained from planar alignment NLC device. Moreover, increasing the spacing between the electrodes again causes the position of this defect to advance further in the  $\gamma$ -direction. Further work is required to investigate how the diffraction efficiency is influenced by the presence of these defects. This could be investigated to design better and sharper gratings profiles.

### Conflict of Interest

The authors declare no conflict of interest.

### Keywords

electric fields, liquid crystals, reconfigurable surfaces

Received: February 24, 2021

Revised: March 9, 2021

Published online:

- [1] T. Wilkinson, C. Henderson, D. Gil Leyva, R. Ghannam, W. Crossland, *Philos. Trans. R. Soc., A* **2006**, 364, 2721.
- [2] J. R. Lindle, A. T. Watnik, V. A. Cassella, *Appl. opt.* **2016**, 55, 4336.
- [3] F. Mok, J. Diep, H.-K. Liu, D. Psaltis, *Opt. Lett.* **1986**, 11, 748.
- [4] W. Crossland, I. Manolis, M. Redmond, K. Tan, T. Wilkinson, M. Holmes, T. Parker, H. Chu, J. Croucher, V. Handerek, et al., *J. Light-wave Technol.* **2000**, 18, 1845.
- [5] J. E. Curtis, B. A. Koss, D. G. Grier, *Opt. Commun.* **2002**, 207, 169.
- [6] Z. Zhang, Z. You, D. Chu, *Light: Sci. Appl.* **2014**, 3, e213.
- [7] C. W. Shields IV, Y.-K. Kim, K. Han, A. C. Murphy, A. J. Scott, N. L. Abbott, O. D. Velev, *Adv. Intell. Syst.* **2020**, 2, 1900114.
- [8] B. Vasić, G. Isić, R. Beccherelli, D. C. Zografopoulos, *IEEE J. Sel. Top. Quantum Electron.* **2019**, 26, 1.
- [9] A. V. Quintero, P. Pérez-Merino, H. D. Smet, *Sci. Rep.* **2020**, 10, 1.
- [10] B. C. Raducanu, S. Zaliasl, S. Stanzione, C. van Liempd, A. V. Quintero, H. De Smet, J. De Baets, C. van Hoof, N. Van Helleputte, *IEEE Solid-State Circuits Lett.* **2020**, 3, 506.
- [11] R. Ghannam, N. Collings, W. Crossland, R. James, S. Day, A. Fernandez, In *Liquid Crystals XI*, vol. 6654. International Society for Optics and Photonics, Bellingham, WA **2007**, p. 66540R.
- [12] R. L. Melcher, *Inf. Disp.* **2000**, 16, 20.
- [13] J. D. Smet, A. Avci, R. Beernaert, D. Cuypers, H. D. Smet, *J. Display Technol.* **2012**, 8, 299.
- [14] A. M. Da Silva, B. Leal, *Seizure* **2017**, 50, 209.
- [15] A. J. Wilkins, A. Baker, D. Amin, S. Smith, J. Bradford, Z. Zaiwalla, F. M. Besag, C. D. Binnie, D. Fish, *Seizure* **1999**, 8, 444.
- [16] M. Yuan, R. Das, R. Ghannam, Y. Wang, J. Reboud, R. Fromme, F. Moradi, H. Heidari, *Adv. Intell. Syst.* **2020**, 2, 1900190.
- [17] N. Hosseinzadeh, M. R. Hesamzadeh, *IEEE Trans. Educ.* **2012**, 55, 495.
- [18] J. Prost, P. S. Pershan, *J. Appl. Phys.* **1976**, 47, 2298.
- [19] R. Lindquist, J. Kulick, G. Nordin, J. Jarem, S. Kowel, M. Friends, T. Leslie, *Opt. Lett.* **1994**, 19, 670.
- [20] E. G. Loewen, E. Popov, *Diffraction Gratings and Applications*, CRC Press, Boca Raton **2018**.
- [21] R. S. Zola, H. K. Bisoyi, H. Wang, A. M. Urbas, T. J. Bunning, Q. Li, *Adv. Mater.* **2019**, 31, 1806172.
- [22] A. Habibpourmoghdam, L. Wolfram, F. Jahanbakhsh, B. Mohr, V. Y. Reshetnyak, A. Lorenz, *ACS Appl. Electron. Mater.* **2019**, 1, 2574.
- [23] T.-H. Choi, J.-W. Huh, J.-H. Woo, J.-H. Kim, Y.-S. Jo, T.-H. Yoon, *Opt. Express* **2017**, 25, 11275.
- [24] T. Choi, J. Woo, J. Baek, Y. Choi, T. Yoon, *IEEE Trans. Electron Devices* **2017**, 64, 3213.
- [25] T.-H. Choi, J.-H. Woo, B.-G. Jeon, J. Kim, M. Cha, T.-H. Yoon, *Liq. Cryst.* **2018**, 45, 1419.
- [26] I. V. Simdyankin, A. R. Geivandov, S. P. Palto, *J. Exp. Theor. Phys.* **2020**, 131, 664.
- [27] H. Chen, G. Tan, Y. Huang, Y. Weng, T.-H. Choi, T.-H. Yoon, S.-T. Wu, *Sci. Rep.* **2017**, 7, 1.

- [28] Y. Garbovskiy, V. Zagorodnii, P. Krivosik, J. Lovejoy, R. E. Camley, Z. Celinski, A. Glushchenko, J. Dziaduszek, R. Dąbrowski, *J. Appl. Phys.* **2012**, *111*, 054504.
- [29] E. Willman, L. Seddon, M. Osman, A. Bulak, R. James, S. Day, F. Fernandez, *Phys. Rev. E* **2014**, *89*, 052501.
- [30] R. Ghannam, N. Collings, W. Crossland, T. Wilkinson, In *Liquid Crystals X*, vol. 6332. International Society for Optics and Photonics, Bellingham, WA **2006**, p. 63320H.
- [31] P.-G. De Gennes, J. Prost, *The Physics of Liquid Crystals*, Vol. 83, Oxford university press, Oxford **1993**.
- [32] N. Mottram, Ph.D. thesis, University of Bristol, **1996**.
- [33] N. Mottram, S. Hogan, *Philos. Trans. R. Soc., A* **1997**, *355*, 2045.
- [34] R. James, E. Willman, F. A. Fernandez, S. E. Day, *IEEE Trans. Electron Devices* **2006**, *53*, 1575.
- [35] E. Willman, F. A. Fernandez, R. James, S. E. Day, *IEEE Trans. Electron Devices* **2007**, *54*, 2630.
- [36] H. Coles, *Mol. Cryst. Liq. Cryst.* **1978**, *49*, 67.
- [37] D. Miroshnychenko, N. Hill, N. Mottram, J. Lydon, *Mol. Cryst. Liq. Cryst.* **2005**, *437*, 251.
- [38] P. Cummins, D. Dunmur, D. Laidler, *Mol. Cryst. Liq. Cryst.* **1975**, *30*, 1-2 109.
- [39] L. M. Blinov, V. G. Chigrinov, *Electrooptic Effects in Liquid Crystal Materials*, Springer Science & Business Media, Berlin **1996**.
- [40] H. Wang, T. X. Wu, X. Zhu, S.-T. Wu, *J. Appl. Phys.* **2004**, *95*, 5502.